Effect of the lanthanide ion on the structure and low-temperature phase transitions in $RbL(SO_4)_2.4H_2O$ (L identical to La-Er) crystals

1992 J. Phys.: Condens. Matter 4 4769

(http://iopscience.iop.org/0953-8984/4/20/004)

J. Phys.: Condens. Matter 4 (1992) 4769–4778. Printed in the UK

Effect of the lanthanide ion on the structure and low-temperature phase transitions in $RbL(SO_4)_2 \cdot 4H_2O$ ($L \equiv$ La–Er) crystals

S Jasty†, V M Malhotra† and P D Robinson‡

† Department of Physics and Molecular Science Program, Southern Illinois University at Carbondale, Carbondale, IL62901-4401, USA

‡ Department of Geology, Southern Illinois University at Carbondale, Carbondale, IL 62901-4401, USA

Received 25 September 1991, in final form 21 February 1992

Abstract. Crystallographic unit cell parameters of $RbL(SO_4)_2 \cdot 4H_2O$ ($L \equiv$ La, Ce, Pr, Nd, Sm, Eu, Gd, Tb, Dy, and Er) are 296 K and specific heat capacity (C_p) data on $RbL(SO_4)_2 \cdot 4H_2O$ ($L \equiv$ Pr, Nd, Sm, Eu, Gd, Tb, Dy, and Er) for $110 < T < 305$ K are presented. The $RbL(SO_4)_2 \cdot 4H_2O$ lattices form an isostructural monoclinic series and have the layered structure of $RbSm(SO_4)_2 \cdot 4H_2O$. The unit cell parameters a, b, c and β reflect an unusual trend with lanthanide size, unlike other isostructural lanthanide series where cell parameters are monotonically related to the lanthanide contraction. The variation in the cell parameters was schematically used to deduce the trend in the buckling of lanthanide–sulphate layers in $RbLSO_4)_2 \cdot 4H_2O$, and it is argued that the observed non-monotonic behaviour in cell parameters is a consequence of this buckling. The C_p measurements indicate that $RbL(SO_4)_2 \cdot 4H_2O$ ($L \equiv$ Pr, Nd, Eu, Gd, Tb and Dy) lattices undergo a λ transition. Additional structural transitions are observed in $RbPr(SO_4)_2 \cdot 4H_2O$, $RbNd(SO_4)_2 \cdot 4H_2O$, and $RbDy(SO_4)_2 \cdot 4H_2O$, while no transitions occur in $RbEr(SO_4)_2 \cdot 4H_2O$ for $110 < T < 305$ K. The lattice stability model, inclusive of the buckling effects, successfully maps the observed trend in T_λ as well as in the order–disorder transition T_2 in isostructural $NH_4L(SO_4)_2 \cdot 4H_2O$ ($L \equiv$ La–Tb) lattices.

1. Introduction

Systems with a layered structure exhibit a variety of interesting properties that can be attributed in part to their pseudo-two-dimensional character. Such systems include intercalated graphite compounds, magnetic systems such as K_2NiF_4, the more recent high-T_c superconducting ceramics, incommensurate systems, and ferroelectrics [1–5]. For some layered crystals, especially those undergoing structural phase transitions, the interactions between the critical variables driving the transitions are to a certain extent topologically restricted to a plane, e.g. perovskite chlorides $(C_nH_{2n+1}NH_3)_2MCl_4$ ($M \equiv$ Mn, Cd and Cu) [6] and stannous chloride dihydrate ($SnCl_2 \cdot 2H_2O$) [7]. For other layered crystals, e.g. the natural mineral colemanite $CaB_3O_4(OH)_3 \cdot H_2O$, the interlayer hydrogen bonds which tie the sheets together are supposedly responsible for the transition [5]. Thus, the interplay between interlayer and intralayer variables appears to dominate the structural stability and phase transition behaviour in layered crystals.

0953-8984/92/204769+10$04.50

Recently a detailed structural analysis of a layered crystal $RbSm(SO_4)_2 \cdot 4H_2O$ (RSMSTH) has been reported [8]. The unit cell is monoclinic with $P2_1/c$ space-group symmetry. The structure consists of a crisscrossing network of Sm coordination polyhedra bridged by sulphate ions along the a and c directions, resulting in layers parallel to the [010] plane. The layers are held together through a system of hydrogen bonds involving the water molecules and sulphate oxygens. It has been found that RSMSTH is isostructural to its ammonium analogue, $NH_4Sm(SO_4)_2 \cdot 4H_2O$ (ASMSTH), though it exhibits a different phase transition behaviour. The ASMSTH lattice is itself a member of an isostructural series [9], having the general formula $NH_4L(SO_4)_2 \cdot 4H_2O$ (ALSTH) with L ≡ La, Ce, Pr, Nd, Sm, Eu, Gd, Tb, and Dy. The specific heat capacity measurements [10] at $130 < T < 300$ K on the ALSTH lattices revealed a unique trend in phase-transition behaviour, quite unlike that observed in other isostructural lanthanide series [11–13]. The lattice stability model, based on the lanthanide size, failed to explain the observed trend in phase-transition temperatures. In an effort to resolve this puzzling trend, it would be interesting to study the phase-transition behaviour of a series such as $RbL(SO_4)_2 \cdot 4H_2O$ (RLSTH), i.e. the rubidium analogue of the ammonium series, ALSTH. This has been undertaken here.

2. Experimental details

Monocrystals of RLSTH were grown by slow evaporation of aqueous solutions containing 4:1 molar ratios of rubidium sulphate and lanthanide sulphate octahydrate at 298 K for L ≡ Pr, Nd, Sm, Eu, Gd, Tb, Dy, and Er, and at 283 K for L ≡ La and Ce [8, 14]. The solution for L ≡ La solution yielded both $RbLa(SO_4)_2 \cdot 4H_2O$ and $RbLa(SO_4)_2$ crystals. The L ≡ Ce solution yielded $RbCe(SO_4)_2 \cdot 4H_2O$, $RbCe(SO_4)_2 \cdot H_2O$ and anhydrous crystals. The anhydrous La and Ce crystals had a morphology different from the tetrahydrate crystals with a whitish appearance. The lack of hydration in these crystals was confirmed by the absence of the vibrational bands of water in the infrared spectrum. Contrary to the observation in [14], our efforts to crystallize $RbTm(SO_4)_2 4H_2O$, irrespective of the alkali-to-lanthanide sulphate ratio used, were unsuccessful.

Clear, prismatic single crystals of approximate dimensions $0.2 \times 0.2 \times 0.1$ mm^3 were selectively picked for the determination of the unit cell parameters. The measurements were made on a Rigaku AFC5S diffractometer with graphite monochromated Mo K_α radiation. A systematic search of reciprocal space over the range $8° < 2\theta < 25°$ yielded 20 reflections. After centring each reflection, a least-squares refinement of the setting angles produced the initial cell constants and the orientation matrix. A Laue check was performed to confirm the crystal symmetry. Final cell constants were obtained from a least-squares refinement of 25 carefully centred, high-intensity reflections in the 2θ range 28°–30°.

The specific heat capacity data on RLSTH at $110 < T < 305$ K were obtained using a well calibrated [8, 10, 15] Perkin–Elmer DSC7 system. The accuracy in temperature was estimated to be ±1 K and was better than 2% in C_p at $135 < T < 305$ K. Since we were unable to extract sufficient quantities of $RbLa(SO_4)_2 \cdot 4H_2O$ and $RbCe(SO_4)_2 \cdot 4H_2O$ crystals from their respective solutions, the specific heat capacity data on RLSTH (L ≡ Pr, Nd, Sm, Eu, Gd, Tb, Dy, and Er) are presented here.

3. Results and discussion

3.1. Crystallographic parameters

Unit cell parameters of the $RbL(SO_4)_2 \cdot 4H_2O$ (RLSTH) crystals with L ≡ La, Ce, Pr, Nd, Sm, Eu, Gd, Tb, Dy, and Er are reproduced in table 1 and represented graphically in figure 1 against the ionic radius [16] of the lanthanide ion. As seen from table 1, the monoclinic cell volume decreases monotonically with the lanthanide ionic radius, evincing that all lattices in the RLSTH series are isostructural and have the $RbSm(SO_4)_2 \cdot 4H_2O$ structure. However, what is interesting is the non-linear behaviour of lattice parameters with the lanthanide ionic radius. Typically, a nominal linear decrease is expected due to the regular lanthanide contraction, as observed for other isostructural lanthanide series [3, 17].

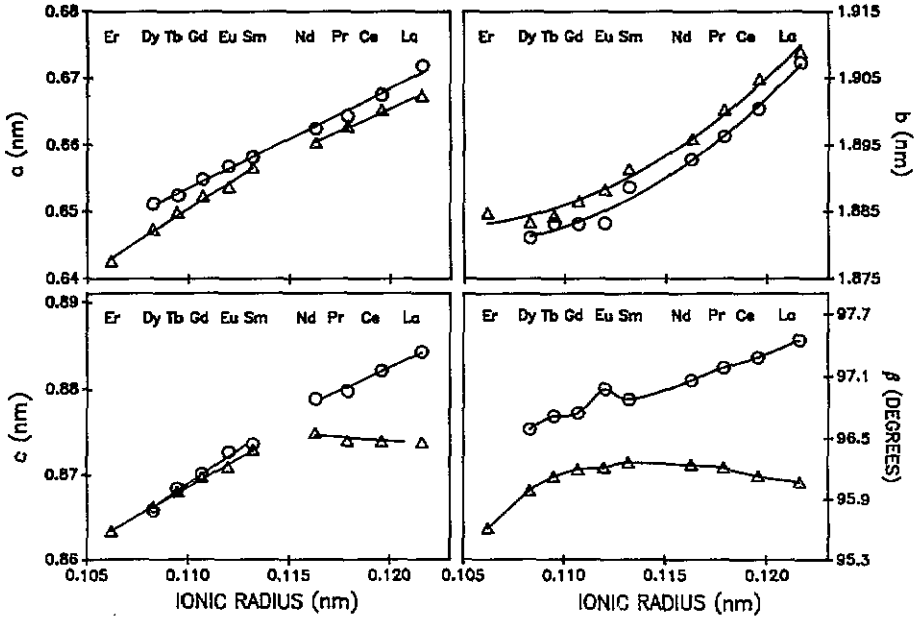

Figure 1. Variation in unit cell parameters with ionic radius of the lanthanide ion for the $RbL(SO_4)_2 \cdot 4H_2O$ (△) the $NH_4L(SO_4)_2 \cdot 4H_2O$ (○) series.

To understand this unusual non-linear behaviour in the unit cell parameters, we recall that the framework of the RLSTH structure consists of lanthanide–sulphate layers parallel to the [010] plane [8]. If the sulphate ions which link adjacent lanthanide ions in the [100] and [001] directions are replaced by solid lines, as presented in figure 2, then it is evident that the layers are not flat but are rather buckled in the [010] direction. Unbuckled or flat layers would imply perfect rigidity against transverse distortion. The relaxation of transverse rigidity of the layers, i.e. buckling, can be quantified in terms of a buckling angle, θ_B ($= (\pi - \phi)/2$). ϕ is the angle between two intersecting planes (segments) in a layer (see figure 2). The various contributions to the unit cell parameters can be schematically represented as

$$u = u_r + u_B + u_o \tag{1}$$

Table 1. Unit cell dimensions for the isostructural rubidium lanthanide sulphate tetrahydrates.[a]

L	Ionic radius[b] (nm)	a (nm)	b (nm)	c (nm)	β^0	Volume $(nm)^3$
La	0.1216	0.6674(4)	1.9089(21)	0.8738(2)	96.07(5)	1.1070(14)
Ce	0.1196	0.6653(8)	1.9048(9)	0.8739(3)	96.13(6)	1.1012(14)
Pr	0.1179	0.6628(8)	1.9003(9)	0.8740(2)	96.21(5)	1.0943(15)
Nd	0.1163	0.6603(3)	1.8959(8)	0.8749(4)	96.24(4)	1.0887(8)
Sm	0.1132	0.6565(2)	1.8913(6)	0.8729(1)	96.26(2)	1.0772(5)
Eu	0.1120	0.6536(3)	1.8881(11)	0.8709(2)	96.21(3)	1.0684(9)
Gd	0.1107	0.6522(2)	1.8864(11)	0.8697(3)	96.19(3)	1.0638(8)
Tb	0.1095	0.6498(3)	1.8843(12)	0.8680(3)	96.12(3)	1.0566(9)
Dy	0.1083	0.6473(4)	1.8833(17)	0.8662(4)	95.98(5)	1.0503(13)
Er	0.1062	0.6426(1)	1.8847(14)	0.8633(2)	95.61(2)	1.0405(8)

[a] Integers in parentheses indicate the estimated error in the least significant digits.
[b] Ionic radii are from [16] for nine-coordinated trivalent lanthanide ions.

where u is an experimentally observed unit cell parameter, i.e. a, b, c; u_r is the contribution to u from the lanthanide ionic radius (r_L); u_B arises from layer buckling; and u_o is due to variables other than ionic radius and buckling. Regular lanthanide contraction requires [13] that $u_r \propto r_L$, while the contribution of u_B to equation (1) is governed by

$$u_B = u_B(\theta_B(r_L)). \tag{2}$$

It is not difficult to see that the cell constant a will remain unaffected to the first order. Also, since the upper and lower layers within a unit cell are not coincident when projected onto the ac plane, but instead are offset by an amount which depends on the magnitude of c, the variation in β with buckling will mimic that in c, i.e. $\beta(\theta_B) \propto c(\theta_B)$. If $\theta_B(r_L)$ is known, then $u_B(r_L)$ can be mapped as a function of r_L. Unfortunately, the detailed structure data for only the RSMSTH lattice are available [8], inhibiting the direct calculation of buckling in each RLSTH lattice.

Since $a_B = 0$ and b_B is correlated to b_o through the interlayer distance, only the variations in c and β would make a contribution to $\theta_B(r_L)$ substantial. As r_L decreases both c_r and c_o will decrease. Consequently, the non-monotonic behaviour in c, depicted in figure 1, must be attributed to a similar non-monotonic trend in $\theta_B(r_L)$. This implies that for the RLASTH structure the layers are highly buckled. For L ≡ Ce, Pr, and Nd, the buckling progressively decreases, reaches a minimum value at L ≡ Nd or Sm ($\theta_B = 48°$ for RSMSTH), and then turns around to progressively increase for L ≡ Eu, Gd, Tb, Dy, and Er.

The observed, unusual non-monotonic trend in $\theta_B(r_L)$ for the RLSTH series can be qualitatively explained in terms of the role played by hydrogen bonding in water toward lattice stability [8]. Of the eight hydrogen bonds donated by the four waters of hydration, two provide intralayer coupling between the lanthanide–sulphate segments shown in figure 2, while six are involved in linking the adjacent layers. As θ_B decreases, the strain on the intralayer and interlayer hydrogen bonds increases. The only means by which the strain on the intralayer hydrogen bonds can be relaxed is when the crisscrossing lanthanide–sulphate chains in each layer will partially absorb the strain by increasing the transverse distortion of the layers. Thus, there is a competition of energies associated with the relaxation of hydrogen bonding geometry

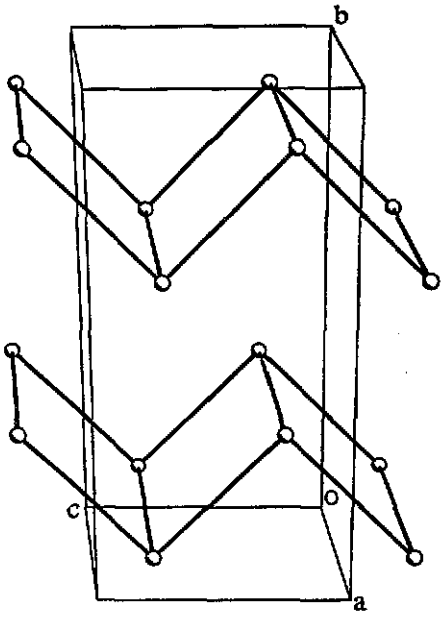

Figure 2. Drawing shows the Sm polyhedron–sulphate layers in $RbSm(SO_4)_2 \cdot 4H_2O$ parallel to the (010) plane and buckled in the b direction. The Sm polyhedra are represented by spheres and the bridging sulphates by full lines.

and transverse layer rigidity. The non-monotonic trend in $\theta_B(r_L)$ suggests that the relaxation of transverse layer rigidity is energetically less demanding and, hence, is favoured over the distortion of hydrogen bonding geometry. From the above discussion, it appears that hydrogen bonding is relatively more important to lattice energy than to less hydrated structures where hydrogen bonds are influenced by steric requirements of the framework [18]. Therefore, hydrogen bonding must play a dominant role in the cohesion of the RLSTH structure. Figure 1 suggests that the unit cell parameters of the ALSTH series display a similar non-monotonic behaviour, though not as pronounced as the RLSTH series.

3.2. Specific heat capacity and phase transitions

The observed specific heat capacity (C_p) curves for the RLSTH lattices with L ≡ Pr, Nd, Sm, Eu, Gd, Tb, Dy, and Er are reproduced in figure 3. The λ-shaped anomaly reported in RSMSTH [8] appears in all the above lattices except RERSTH. In fact, the C_p curve of RERSTH shows no anomalies, indicating the absence of any structural phase transition in this lattice at $100 < T < 305$ K. It is worth noting that RERSTH and ADYSTH [10], both of which are the last members of their respective RLSTH and ALSTH series, undergo no phase transitions. Besides the λ anomaly, the C_p curves of RPrSTH and RNdSTH show an additional, sharp, low-temperature anomaly typical of first-order transitions. The corresponding transition temperatures are arbitrarily denoted T_1. For RNdSTH, an additional step-like anomaly occurs at 249 K, manifesting a third transition of second or higher order. A similar transition at a temperature above the λ transition, but very close to it, appears in the RDYSTH lattice, as seen from

the two closely juxtaposed peaks in its C_p curve (see figure 3). These higher-order transition temperatures are arbitrarily denoted T_3.

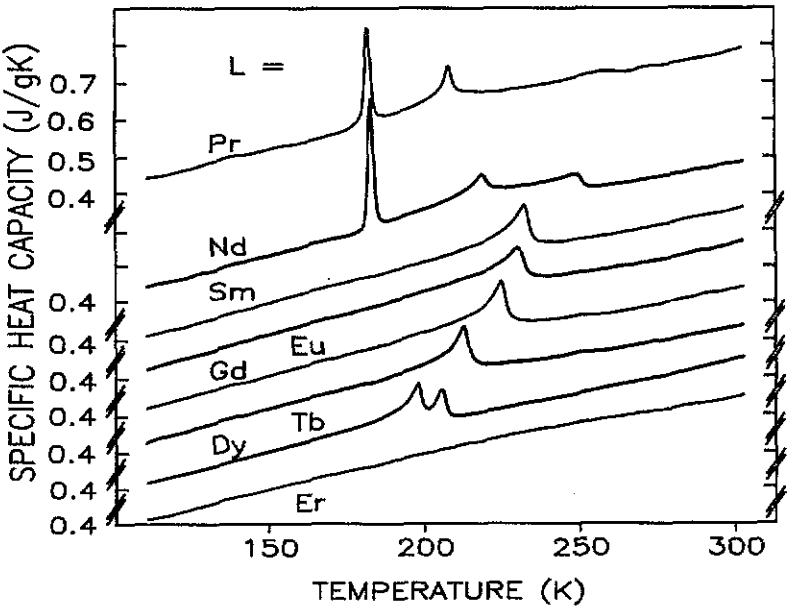

Figure 3. The observed specific heat capacity of $RbL(SO_4)_2{\cdot}4H_2O$ (L ≡ Pr, Nd, Sm, Eu, Gd, Tb, Dy and Er) at $100 < T < 305$ K. The curves have been displaced vertically for comparison and clarity, and the ordinate scale is the same for all curves.

The observed transition temperatures for RLSTH (L ≡ Pr, Nd, Sm, Eu, Gd, Tb, and Dy) lattices are listed in table 2. The enthalpies and entropies associated with the T_1, T_λ and T_3 transitions are also summarized in table 2. They were estimated by using the featureless C_p curve of RERSTH to simulate the background specific heat capacity of the other RLSTH lattices in which transitions occur.

Table 2. Transition temperatures, enthalpies and entropies of the structural phase transitions in isostructural $RbL(SO_4)_2{\cdot}4H_2O$ lattices with accuracies of (±1 K), (±0.01 J g^{-1}) and (±0.0002 J g^{-1} K^{-1}), respectively.

	Transition temperature (K)			Transition enthalpy (J g^{-1})			Transition entropy (J g^{-1} K^{-1})		
L	T_1	T_λ	T_3	ΔH_1	ΔH_λ	ΔH_3	ΔS_1	ΔS_λ	ΔS_3
Pr	182	208		0.75	0.60		0.0041	0.0029	
Nd	183	219	249	0.81	0.39	0.16	0.0045	0.0018	0.0006
Sm		232			1.41			0.0061	
Eu		230			1.35			0.0059	
Gd		225			1.26			0.0056	
Tb		213			1.04			0.0048	
Dy		198	206		0.67	0.38		0.0035	0.0019

Figure 4 depicts the dependence of T_λ on the ionic radius (r_L) of the lanthanide ion. It can be seen from this graph that T_λ increases as r_L decreases, reaches a

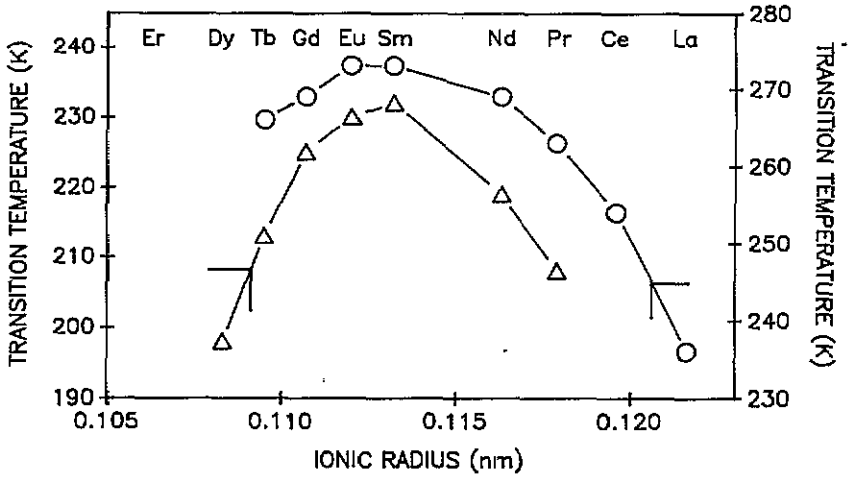

Figure 4. Effect of the lathanide ionic radius on the λ transition temperature in isostructural $RbL(SO_4)_2 \cdot 4H_2O$ (Δ) and on the order–disorder transition T_2 in isostructural $NH_4L(SO_4)_2 \cdot 4H_2O$ (O). The data for the ammonium series is from [10].

maximum for L = Sm, and then decreases with a further decrease in the lanthanide ion size. This trend is similar to that observed for the transition temperature T_2 in the ALSTH series [10] (figure 4). It was inferred above from the trends in the crystallographic parameters that the variation in buckling, θ_B, is non-monotonic as a function of r_L, with the inflection point at $L \equiv Sm$. Clearly, there is an inverse correlation between the T_λ and θ_B trends, suggesting that the λ transition is related to the buckling of the layers.

In order to extend the lattice stability model [19] to include the buckling effect, we note that the trend in buckling ($\theta_B(r_L)$) is a direct consequence of the critical role played by the water molecules' hydrogen bonding toward lattice stability of the room-temperature phase. At the inflection point $L \equiv Sm$, where the buckling of the layers reaches a minimum, the distortion of the hydrogen bonding geometry must be a maximum. If we assume that the λ transition is triggered by the hydrogen bonding of water, then the room-temperature phase should be least stable for RSMSTH. Correspondingly, its T_λ should be highest; while T_λ for lattices with lanthanide ions larger and smaller than Sm should be lower. This follows since the lanthanide–sulphate layers in these lattices are more buckled, leading to less distortion of the H bonding geometry. Since the observed variation in T_λ is consistent with the predicted trend, it can be argued that the water molecules may be playing an important role in triggering the λ transition in RLSTH lattices.

The hydrogen bonding scheme proposed [8] for the water molecules in ASMSTH at 296 K included two alternative acceptors for O(W(1)) and O(W(3)). Since the corresponding distances [O(W(3)), O(1)] = 0.316 nm and [O(W(1)), O(W(1))] = 0.323 nm are longer than, though close to, the upper limit (0.31 nm) for hydrogen bonds of this kind, they were considered weak contacts rather than true hydrogen bonds. In light of the above discussion for the λ transition, it is conceivable that certain hydrogen atoms have two possible positions of equilibrium in the high-temperature phase. Thus, the λ anomaly could be the result of an order–disorder transition induced as a consequence

of fluctuations of water dipoles [20, 21] or as a consequence of the initiation of proton tunnelling between hydrogen-bonded water molecules, e.g. [O(W(4))—O(W(3))] or [O(W(1))—O(W(1))] [5, 22]. Specific heat capacity data alone cannot distinguish between the two types of order–disorder transitions.

To probe the critical behaviour near the λ transition in RLSTH, we attempted to fit the specific heat capacity data to a logarithmic function [8, 10, 15, 23, 24], i.e.

$$C_p = A(\ln \epsilon) + B \tag{3}$$

and a power law, i.e.

$$C_p = A'\epsilon^{\alpha} + B' \tag{4}$$

where ϵ is the reduced temperature, $|(T/T_\lambda) - 1|$. Logarithmic behaviour was observed over nearly two decades in ϵ in the critical regions, $\epsilon < 0.05$ for $T < T_\lambda$ and $\epsilon < 0.02$ and $T > T_\lambda$. Regression coefficients varied between 0.97 and 0.99. As for the T_2 transition in ALSTH [10] lattices, the specific heat capacity data in RLSTH could also not be fitted by a power law over reasonable ranges of ϵ. The nearly identical critical behaviour at T_λ and T_2 transitions in RLSTH and ALSTH, respectively, strongly suggests that the driving mechanism for both transitions is the same.

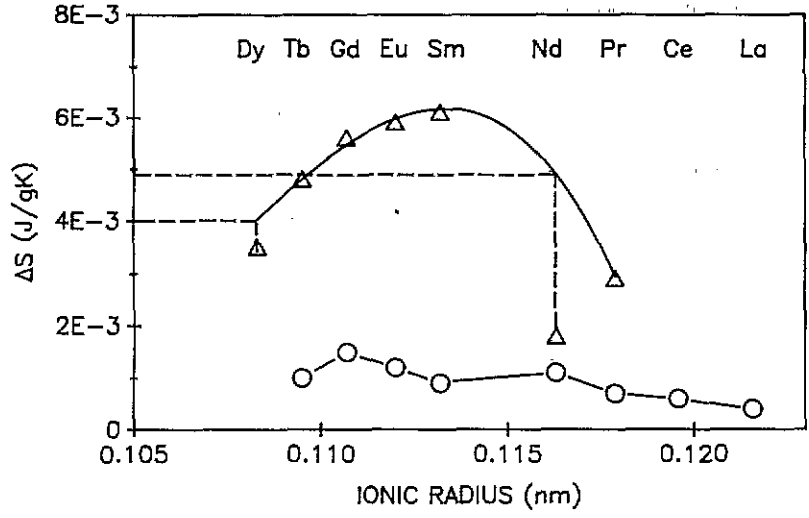

Figure 5. Trend in the λ transition's entropy as a function of the lanthanide size for isostructural $RbL(SO_4)_2 \cdot 4H_2O$ (Δ), while open circles (○) show similar data for T_2 in $NH_4L(SO_4)_2 \cdot 4H_2O$. The data for the ammonium series are from [10]. The broken lines (– – –) indicate the graphically estimated values of ~ 0.005 J g^{-1}K^{-1} for $RbNd(SO_4)_2 \cdot 4H_2O$ and ~ 0.004 J g^{-1}K^{-1} for $RbDy(SO_4)_2 \cdot 4H_2O$, which are higher than the observed values.

Figure 5 delineates the dependence of the observed entropies (ΔS_λ) associated with the λ transition in RLSTH on the ionic radius of the lanthanide. The same general trend that was observed for T_λ is also seen for ΔS_λ. Again. like T_λ, the maximum of ΔS_λ occurs at RSMSTH. The λ transition, as argued earlier, is induced

by hydrogen bonds, affecting a rearrangement from the ordered low-temperature phase to the disordered room-temperature phase in the RSMSTH lattice. Therefore, it will require the largest entropy. Moreover, the variation in ΔS_λ should be the inverse of the buckling trend which is almost consistent with the observed behaviour, shown in figure 5. There are two exceptions to this trend. For RNdSTH and RDYSTH, ΔS_λ deviates from the graphically predicted values of ~ 0.0050 J $g^{-1}K^{-1}$ and ~ 0.0040 J $g^{-1}K^{-1}$, respectively. However, for these two lattices a higher-order transition at $T_3 > T_\lambda$ occurs. We therefore argue that in RNdSTH and RDYSTH the λ transition results in only a partial disordering of the water dipoles or protons. The disordering is then completed via the T_3 transition.

For the ALSTH series, the entropies associated with the T_2 transitions [10], ΔS_2, plotted in figure 5, are almost an order of magnitude smaller than the value of ΔS_λ. This is in agreement with the conclusion that hydrogen bonding of water is more important for the stability of the RLSTH structure than for the ALSTH structure [8].

4. Summary

We have determined the unit cell parameters of the $RbL(SO_4)_2 \cdot 4H_2O$ ($L \equiv$ La, Ce, Pr, Nd, Sm, Eu, Gd, Tb, Dy, and Er) series and have investigated the phase transitions' behaviours of the lattices (except for La and Ce) at $100 < T < 305$ K. The non-linear trends in the cell constants indicate that the variation in buckling of the lanthanide–sulphate layers is approximately described by an asymmetric V shape with respect to the lanthanide ionic radius. This non-monotonic buckling trend is a consequence of the importance of the hydrogen bonding of water to the lattice energy. The inverse correlation between the variations in the transition temperatures, T_λ, and in the buckling with lanthanide ionic radius implies that the λ transition is induced by fluctuations of water dipoles or by the initiation of proton tunnelling between hydrogen-bonded water molecules.

References

[1] Thorpe M F, Jin W and Mahanti S D 1989 *Phys. Rev.* B **40** 10 294
[2] Parsonage N G and Stavely L A K 1978 *Disorder in Crystals* (Oxford: Clarendon)
[3] Buchner B, Callieb U, Jostarndt H D, Schlabitz W and Wohlleben D 1990 *Solid State Commun.* **73** 357
[4] Monctor D E, Axe J D and DiSalvo F J 1975 *Phys. Rev. Lett.* **34** 734
[5] Jona F and Shirane G 1962 *Ferroelectric Crystals* (New York: Pergamon)
[6] Borsa A and Rigamonti F 1979 *Magnetic Resonance of Phase Transitions* ed F J Owens, C P Poole and H A Farach (New York: Academic) pp 79–164
[7] Banerjee S, Nath D and Chaudhuri B K 1982 *Phys. Rev.* B **25** 1883
[8] Jasty S, Robinson P D and Malhotra V M 1991 *Phys. Rev.* B **43** 13 215
[9] Eriksson B, Larsson L O, Niinisto L and Skoglund U 1974 *Inorg. Chem.* **13** 290
[10] Jasty S and Malhotra V M 1992 *Phys. Rev.* B **45** 1
[11] Weber H P, Tofield B C and Liao P F 1975 *Phys. Rev.* B **11** 1152
[12] Poole C P Jr, Farach H A and Creswick R J 1987 *Ferroelectrics* **71** 143
[13] Vrtis M L, Jorgensen J D and Hinks D G 1990 *J. Solid State Chem.* **84** 93
[14] Iskhakova L D and Plyushchev V E 1973 *Russ. J. Inorg. Chem.* **18** 790, and references therein
[15] Mu R and Malhotra V M 1991 *Phys. Rev.* B **44** 4296
[16] Shannon R D 1976 *Acta Crystallogr.* A **32** 751
[17] Brixner L H, Bierstedt P E, Sleight A W and Licis M S 1971 *Mater. Res. Bull.* **6** 545

[18] Baur W H and Khan A A 1970 *Acta Crystallogr.* B **26** 1584
[19] Scott J F and Remeika J P 1970 *Phys. Rev.* B **1** 4182
[20] Malhotra V M, Buckmaster H A and Bist H D 1980 *Can. J. Phys.* **58** 1667
[21] Buckmaster H A, Malhotra V M and Bist H D 1981 *Can. J. Phys.* **59** 596
[22] Fleury P A and Lyons K 1981 *Structural Phase Transitions I (Springer Topics in Current Physics 23)* ed K A Muller and H Thomas (New York: Springer) pp 10–89
[23] Fecht H J, Fu Z and Johnson W L 1990 *Phys. Rev. Lett.* **64** 1753
[24] Cheung K M and Ullman F G 1974 *Phys. Rev.* B **10** 4760